

Combined Funnel, Concentrator, and Particle Valve Functional Element for Magnetophoretic Bead Transport Based on Engineered Magnetic Domain Patterns

Rico Huhnstock,* Lukas Paetzold, Maximilian Merkel, Piotr Kuświk, and Arno Ehresmann*

Controlled actuation of superparamagnetic beads (SPBs) within a microfluidic environment using tailored dynamic magnetic field landscapes (MFLs) is a potent approach for the realization of point-of-care diagnostics within Lab-on-a-chip (LOC) systems. Making use of an engineered magnetic domain pattern as the MFL source, a functional LOC-element with combined magnetophoretic “funnel”, concentrator, and “valve” functions for micron-sized SPBs is presented. A parallel-stripe domain pattern design with periodically decreasing/increasing stripe lengths is fabricated in a topographically flat continuous exchange biased (EB) thin film system by ion bombardment induced magnetic patterning (IBMP). It is demonstrated that, upon application of external magnetic field pulses, a fully reversible concentration of SPBs at the domain pattern’s focal point occurs. In addition, it is shown that this functionality may be used as an SPB “funnel”, allowing only a maximum number of particles to pass through the focal point. Adjusting the pulse time length, the focal point can be clogged up for incoming SPBs, resembling an on/off switchable particle “valve”. The observations are supported by quantitative theoretical force considerations.

1. Introduction


Superparamagnetic beads (SPBs) are discussed as central components of future point-of-care diagnostic and analytic devices,^[1–3] realized in micro-total-analysis-systems (μ TAS) or lab-on-a-chip (LOC) devices.^[4–6] They are available in different sizes, compositions, and chemical surface functionalizations, enabling specific analyte binding and isolation from a screened fluid.^[7,8] SPB-based biodetection schemes discussed in literature rely on the particles’ remotely-controllable actuation. A major strategy for actuation is the use of local field gradients within tailored magnetic stray field landscapes (MFLs) emerging from a chip substrate superposed by a dynamically varying external magnetic field.^[9–13] These MFLs have been created by periodic arrays of micro-structured soft-/hardmagnetic elements^[9,14–17] or by magnetic domains in full magnetic thin film systems,^[10,18–21] the latter either

occurring naturally in ferromagnetic garnet films^[18] or artificially tailored by magnetic patterning of continuous exchange bias (EB)^[10,20,22,23] or multilayer^[24] thin film systems. Prominent examples of magnetic patterning techniques for EB thin film systems are ion bombardment induced magnetic patterning (IBMP),^[23] thermally assisted scanning probe lithography,^[25] and laser-based direct-writing.^[26] The MFL’s steep magnetic field gradients between adjacent field minima and maxima (typically separated by a few μm) yield comparably high SPB steady-state transport velocities with more than $100 \mu\text{m s}^{-1}$.^[12,18,27]

An important functionality of dynamic MFLs suitable for LOC devices is their ability to guide SPBs toward a sensing position in order to increase analyte detection sensitivity,^[28] thus, emphasizing the need for a matching micromagnetic pattern within the underlying substrate. For instance, conducting micro-loops,^[29,30] spiderweb-like,^[28] concentric cylinder^[31] as well as periodic circular micromagnetic structures^[32] have been utilized to controllably focus SPBs toward a designated on-chip area, either with the goal of detecting the particles^[28,29,32] or reducing the interparticle distance for a potential analyte-induced particle aggregation.^[31] However, lacking control over the number of SPBs arriving at the focus position is oftentimes a drawback: Typically, all

R. Huhnstock, L. Paetzold, M. Merkel, A. Ehresmann
Institute of Physics and Center for Interdisciplinary Nanostructure
Science and Technology (CINSaT)
University of Kassel
Heinrich-Plett-Str. 40, D-34132 Kassel, Germany
E-mail: rico.huhnstock@physik.uni-kassel.de;
ehresmann@physik.uni-kassel.de

R. Huhnstock, L. Paetzold, M. Merkel, A. Ehresmann
Artificial Intelligence Methods for Experiment Design (AIM-ED)
Joint Lab of Helmholtzzentrum für Materialien und Energie
Berlin (HZB) and University of Kassel
Hahn Meitner-Platz 1, D-14109 Berlin, Germany
P. Kuświk
Institute of Molecular Physics
Polish Academy of Sciences
M. Smoluchowski 17, Poznań 60–179, Poland

 The ORCID identification number(s) for the author(s) of this article can be found under <https://doi.org/10.1002/small.202305675>

© 2023 The Authors. Small published by Wiley-VCH GmbH. This is an open access article under the terms of the Creative Commons Attribution License, which permits use, distribution and reproduction in any medium, provided the original work is properly cited.

DOI: 10.1002/small.202305675

particles subjected to the MFL above the micromagnetic pattern will be focused, resulting in a broad distribution for the number of assembled particles. A defined number of particles would be beneficial when combining the focusing step with magnetoresistive particle detection^[29,30,33] since the measured signal could be directly used for sensor calibration. In case of analyte-induced SPB aggregation, no regulation of the number of incoming particles would accordingly lead to no control over the aggregate sizes, which especially hinders the quantification of analyte concentrations in such detection assays. Additionally, analyte detection based on particle aggregation typically combines two steps: First, bead aggregation has been induced by a permanent magnet prior to on-chip handling, accumulating beads close to the magnet and, thus, enhancing the probability of binding events.^[32,34,35] Then, in a second step, analyte-bridged SPBs have been separated from single ones by non-linear magnetophoresis in dynamically varying MFLs.^[32,34] This concept of analyte-induced SPB aggregation has been showcased for the detection of the model protein biotinylated bovine serum albumin,^[34] double-stranded DNA,^[34] the herpes simplex virus (HSV)-1^[35] as well as the HSV-related gene UL27.^[32] It is therefore a viable approach for point-of-care testing, involving so far, however, no microscopic control over the aggregates' size and shape owing to the macroscopic field of a permanent magnet used for bead aggregation.

Overcoming these downsides, we have designed in this work a functional element with tailored MFL, which, in combination with a superposed dynamically varying external field fulfills two necessities: 1.) Limitation of the amount of transported SPBs toward a focusing region and 2.) combination of the two steps of (I) bead approach for potential analyte-binding-induced aggregation and (II) separation of beads after their approach in a continuous motion cycle. Starting from a prototypical IBMP-engineered parallel-stripe domain pattern with periodically alternating head-to-head (hh)/ tail-to-tail (tt) magnetization configurations,^[10,20] the stripe lengths have been gradually varied for the presented study, creating a “magnetophoretic funnel” for laterally transported SPBs. Decreasing the stripe domain length, while keeping the width constant, shortens the trapping sites for SPBs in one dimension, consequently bringing the particles closer to each other (**Figure 1a**). Lowered interparticle distances are expected in this case because a reduced stray field strength for shorter domain walls (DWs) weakens the dipolar repulsion between single SPBs. Additionally, fringe fields at the upper/lower boundaries of magnetic stripe domains in γ -direction should further stabilize SPB formations with reduced interparticle distances. This has two effects: On the one hand, the relation of SPB size and DW length allows only for a limited number of SPBs passing through during lateral particle transport. On the other hand, reduced distances between single SPB are expected to enhance the probability of analyte-binding-induced aggregation in future detection assays. Demonstrating our capability to reversibly increase the interparticle distance and therefore dissolve SPB aggregates without analyte bridges, the DW length is gradually increased beyond the focal point of the pattern. It is expected that SPBs will be well separated again in this region since dipolar repulsion between SPBs is becoming more pronounced due to parallelly aligned magnetic moments^[10] and increasing stray field strengths. As a proof-of-principle of the discussed advantages, we experimentally test the lateral transport of SPBs without surface functionaliza-

tion, correlating the SPB motion dynamics observed by an optical bright-field microscope with the tailored magnetic domain pattern imaged *via* magnetic force microscopy (MFM) as well as with numerical simulations for the resulting MFL and the acting forces on the particles. By varying the time length of externally applied magnetic field pulses, we will additionally demonstrate that beyond a critical threshold the “magnetophoretic funnel” can be jammed for incoming SPBs, adding a particle “valve” functionality to the utilized domain pattern.

2. Results

2.1. Magnetic Domain Pattern And Magnetic Stray Field Landscape

Magnetic parallel-stripe domain patterns with periodically decreasing and increasing stripe lengths were fabricated within EB thin film systems *via* IBMP (see Figure S1, Supporting Information for an image of the utilized resist structure). The stripes of 5 μm width and remanent in-plane magnetization along their short axes are hereby embedded in a monodomain phase of opposite magnetization direction in remanence. The length of the stripes was varied between 5 and 50 μm with an increment of 5 μm , i.e., the vertical distance between upper/lower edges of consecutive stripes amounts to 2.5 μm . To confirm the successful fabrication of the domain pattern and to investigate occurring DW types, MFM measurements were performed for an exemplary sample area of 80 $\mu\text{m} \times 80 \mu\text{m}$ with a tip elevation of 200 nm above the substrate. The result is shown in Figure 1b, with the MFM phase signal represented by a pseudocolor. Here, DWs between stripe domains and the surrounding monodomain environment are clearly visible as regions with the darkest (right boundary of a stripe) and lightest (left boundary of a stripe) phase signal contrast. As the stripe domains are antiparallely magnetized with respect to their environment (indicated by blue arrows) three different DW configurations can be identified: hh, tt, and side-by-side (ss). Each of the corresponding DWs carries a different magnetic charge distribution profile, resulting in different strengths for the emerging magnetic stray fields.^[36]

To study the theoretical MFL emerging from this domain pattern, micromagnetic simulations, using the MuMax3 software package,^[37] were performed for the sample area marked by the black rectangle in Figure 1b. The used simulation parameters and dimensions can be found in the Methods section. From the obtained distribution of magnetic moments \vec{m} , magnetic stray fields at position $\vec{r}(x, y, z)$ were calculated according to the dipole approximation:^[38]

$$\vec{H}(\vec{r}) = \frac{1}{4\pi} \cdot \sum_i \frac{3 \cdot (\vec{R} \cdot \vec{m}_i) \cdot \vec{R}}{|\vec{R}|^5} - \frac{\vec{m}_i}{|\vec{R}|^3} \quad (1)$$

Within this formula, $\vec{R} = \vec{r} - \vec{r}_i$ denotes the distance vector between spatial position \vec{r} and dipole position \vec{r}_i . The different MFL components H_z , H_x , and H_y in z -, x -, and y -direction were computed at a distance of 1600 nm above the substrate surface and are depicted as pseudocolor plots in Figure 1c.

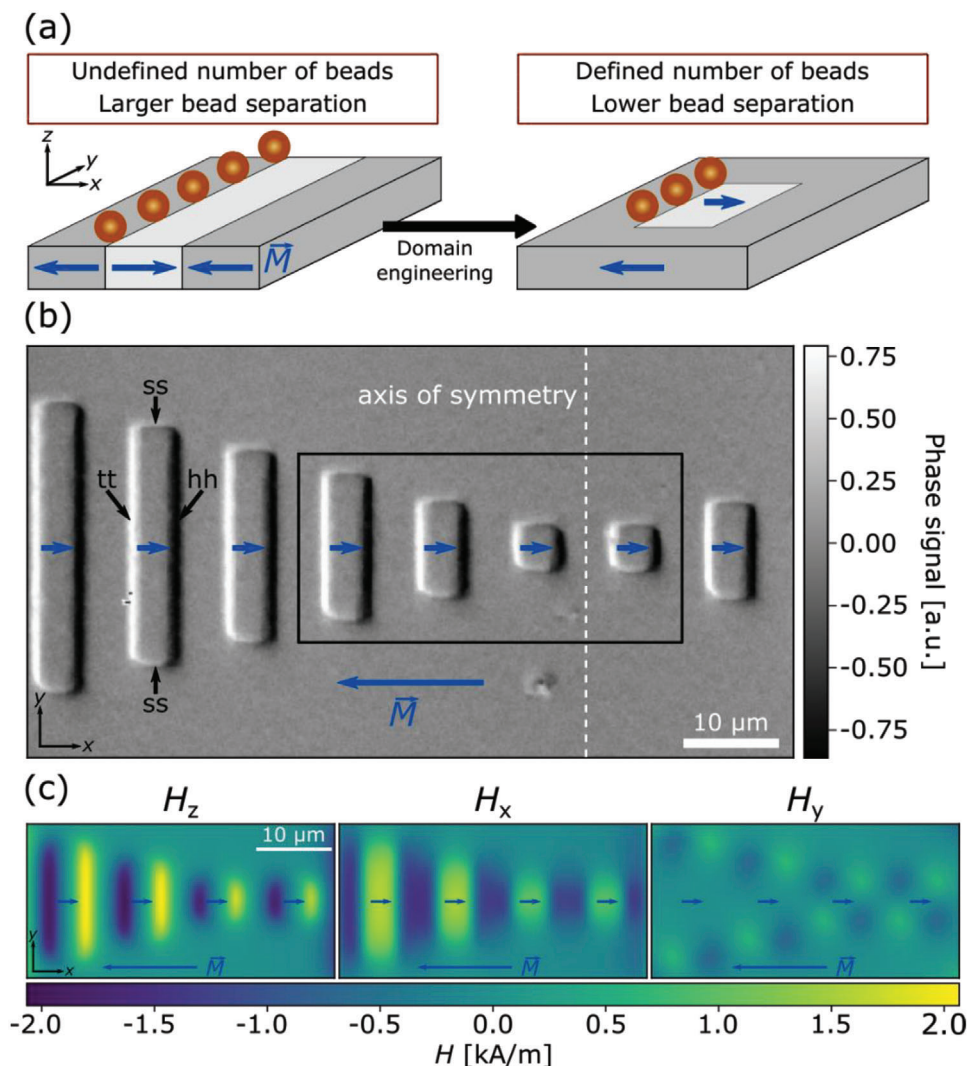


Figure 1. Designed magnetic parallel-stripe domain pattern with gradually decreasing/increasing length for controlled funneling and accumulation of SPBs. a) Schematic concept for limiting the number of accumulated SPBs achieved by the engineering of magnetic stripe domains. The DWs act as trapping sites for SPBs, thereby leading in addition to a decrease in the interparticle distance with decreasing stripe length. b) Phase contrast MFM image at an elevation of $z = 200$ nm above the substrate. Light and dark gray levels mark positions of DWs. Gray level changes across DWs indicate head-to-head (hh), tail-to-tail (tt), or side-by-side (ss) DWs.^[23,36] The axis of symmetry is indicated at which the domain pattern is mirrored. c) Simulated MFL at an elevation $z = 1600$ nm above the magnetic substrate for the region of interest signified by the black frame in (b). Shown are the magnetic field components H_z , H_x , and H_y as a function of position, respectively.

The elevation of 1600 nm was chosen due to the radius of investigated SPBs being 1400 nm and the thickness of a Poly(methyl methacrylate) (PMMA) spacing layer on top of the magnetic thin film system being 200 nm, thus, the MFL was simulated at the approximated position of physical particle centers above the substrate, which is expected to coincide also with the magnetic center of the SPBs. Computed stray fields can, therefore, be used to estimate the magnitude of magnetic forces acting on the studied SPBs. As can be seen from Figure 1c, maximum magnitudes for $|H_z|$ are found directly at the positions of DWs with hh and tt magnetization configuration of adjacent domains. On the contrary, maximum $|H_x|$ occurs between hh and tt DWs, i.e., either above a stripe domain or above the gap between two stripe domains. As a common feature for H_z and H_x distribu-

tions, the magnetic field magnitude is predicted to be lowered above the smallest stripe domains of 5 μm length compared to stripe domains with larger lengths. For instance, maximum $|H_z|$ is 2.05 kA m^{-1} for DWs of 10 μm length and 1.74 kA m^{-1} for 5 μm DWs according to the simulation results. This trend proves to be vital for finding a physical explanation for the herein-discussed SPB concentrator and “valve” functionalities of the magnetic domain pattern (see the Discussion section for a more detailed theoretical analysis). Examining the computed distribution of H_y , alternating maxima/minima can be identified at the corners of each stripe domain. These fringe fields are expected to play a crucial role in the funneling and concentration of SPBs described below. Compared to H_z however, the maximum magnitude $|H_y|$ is approximately only 30% of maximum $|H_z|$. Judging solely from

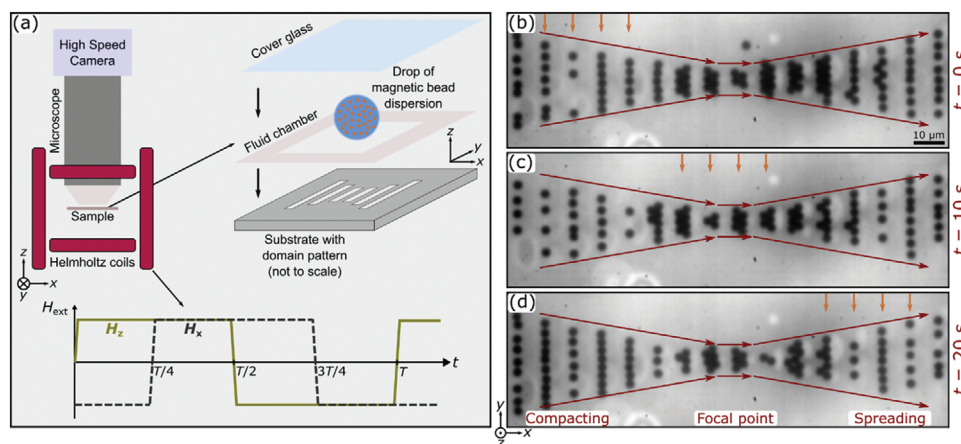


Figure 2. Directed transport of SPBs on top of a magnetic parallel-stripe domain pattern with gradually decreasing/increasing stripe lengths. a) Sketches for the experimental setup used within this study, consisting of a microfluidic chamber assembled above the domain pattern containing substrate. A volume of aqueous SPB dispersion is added to this chamber and SPB motion dynamics are initiated after a short sedimentation time by periodically applying the shown sequence of external magnetic fields in x - and z -direction (H_x/H_z). The motion is captured via an optical bright-field microscope attached to a high speed camera (1000 fps recording rate). Spatial positions and formations of the SPBs (black spots) are displayed exemplarily for experimental times of b) $t = 0$ s, c) $t = 10$ s, and d) $t = 20$ s. A transformation of SPB row formations into clustered formations upon reaching the domain pattern's focal point and vice versa is highlighted by following four SPB assemblies throughout panels (b–d) with brown arrows.

these magnetic stray field strengths, SPBs situated above the substrate should be primarily attracted toward the positions of DWs with hh and tt magnetization configurations.

2.2. SPB Motion Dynamics

2.2.1. Funnel and Concentrator Functionality

The experimental setup used for initializing and recording SPB motion dynamics is sketched out in **Figure 2a**. An aqueous dispersion of SPBs (Dynabeads M-270) with a diameter of $2.8 \mu\text{m}$ was placed on top of the magnetically patterned substrate, contained by a fluid chamber as well as a cover glass. Similar to previous works,^[10,12,13,27] a one-directional, stepwise transport of the particles was initialized by making use of Helmholtz coils to apply a periodic sequence of external trapezoidal magnetic field pulses in z - and x -direction with magnitudes of $\mu_0 \cdot H_{z,\text{max}} = \mu_0 \cdot H_{x,\text{max}} = 1 \text{ mT}$ (μ_0 being the vacuum permeability). This strength of the external field pulses was chosen in order to be in the range of maximum MFL magnitudes and to simultaneously avoid remagnetization of the magnetic substrate. One period of the applied sequence for H_z (olive) and H_x (gray dashed) is schematically visualized in **Figure 2a**. The field direction is hereby alternating periodically and both sequences for z - and x -direction are separated by a phase shift of $\pi/2$. Recording the ensuing SPB motion with a high speed camera (1000 frames per second) attached to an optical bright-field microscope, exemplary snapshots are shown in **Figure 2** for experimental times of $t = 0$ s (b), $t = 10$ s (c), and $t = 20$ s (d). For this experiment, a period $T = 2$ s was chosen for the external magnetic field sequence.

As indicated by the red arrows, the particles are moving from the left to the right of the chosen field of view and their positions closely resemble the decreasing and subsequently increasing length of magnetic stripe domains in the underlying sub-

strate. It is observed that formations of SPBs are compacted with respect to the y -dimension upon moving to the sample position of smallest stripe domain length (here denoted as the focal point), with a spreading of the particles occurring once they moved through the focal point and reached stripe domains of increasing length. SPBs are situated within vertical rows on the substrate areas left and right from the focal point, i.e., positions of increasing stripe domain length (see brown arrows in **Figure 2b**). Here, the SPB arrangement is comparable to results for magnetic parallel-stripe domain patterns where the stripe length is equal to the substrate size.^[10] When interacting with the MFL that is superposed with the external field, minima for the SPBs' potential energy are present above the DWs with either hh or tt magnetization configuration,^[10] leading to the capture of the particles at these positions.

Shifting these potential energy minima *via* the periodic external magnetic field pulses results ultimately in the movement of the SPBs along the x -direction (Video S1, Supporting Information). As the magnetic moments of the SPBs are aligned along the effective magnetic field and therefore in a parallel configuration,^[10] particles are repelling each other when being situated within the observed row formation. This situation changes when the SPBs move toward the focal point: If more than two particles arrive simultaneously at this position, a transition to a clustered formation is observed where particles are arranged in a zigzagging chain (see brown arrows in **Figure 2c**). The transformation is already initiated before the focal point since single particles are ejected to the sides of a row formation when the physical space above a DW is not sufficient for all SPBs present. Interestingly, the arrangement of SPBs is reversibly transformed back to the row formation upon reaching the sample area with increasing stripe domain lengths (highlighted by brown arrows in **Figure 2d**). As a first implication, the observed reversible and stepwise switching between clustered and row formation of SPBs means that the interparticle

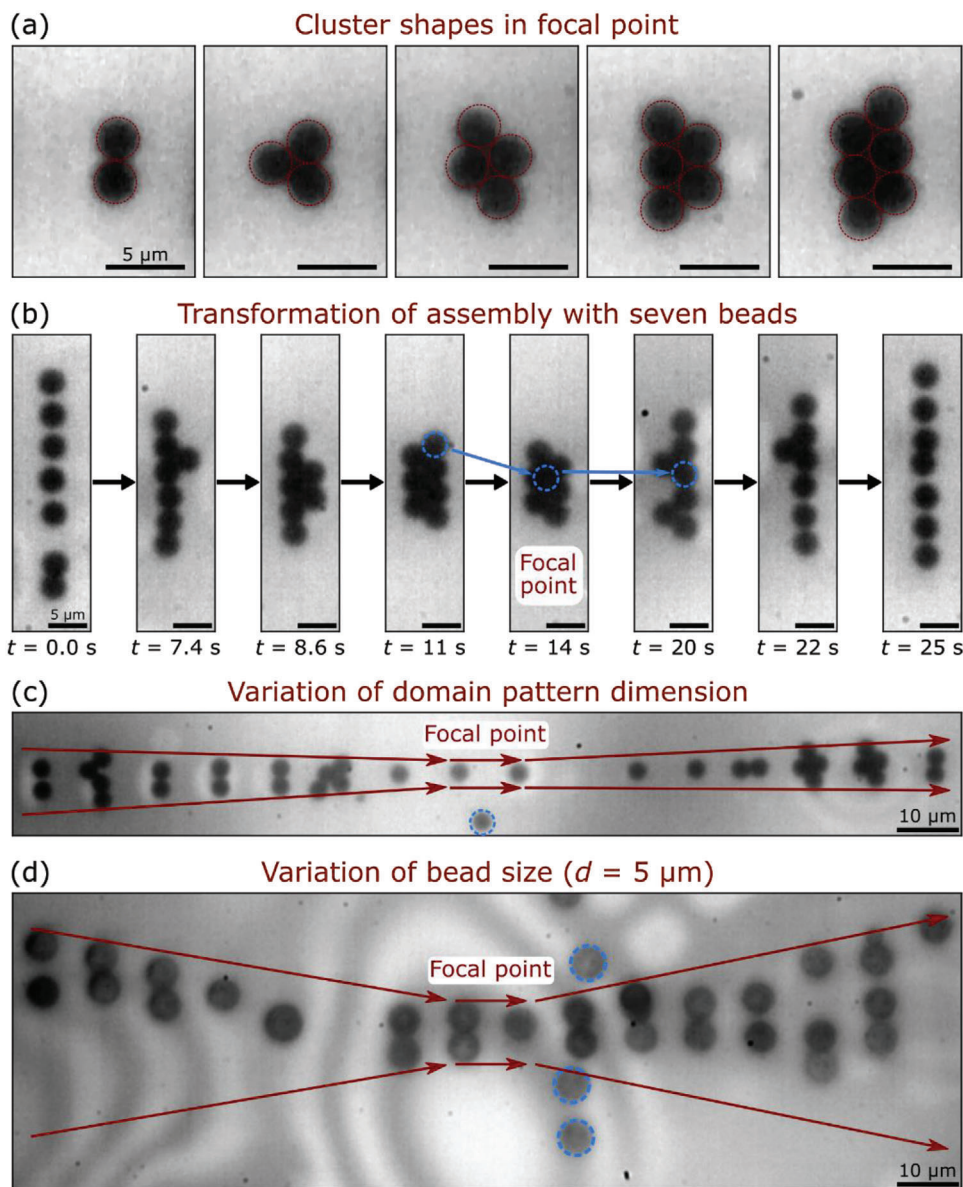


Figure 3. Controlling the shape and size of induced SPB cluster formations. a) Microscope images showing the assembly of two, three, four, five, and six SPBs, respectively, into cluster formations within the focal point of the underlying domain pattern. Single SPBs (highlighted by red circles) are in close physical contact with each other for each observed formation. b) Approach and retreat of a seven SPB formation with respect to the domain pattern's focal point. It was observed that a surplus bead (indicated by blue circles) could be stacked on top of the remaining bead assembly within the focal point so that it jumps back into the row formation for increased stripe domain length. c) SPB cluster formations observed for a domain pattern of similar structure but smaller stripe domain length in the focal point ($2\ \mu\text{m}$). d) SPB cluster formations observed for the mainly discussed domain pattern ($5\ \mu\text{m}$ minimal stripe domain length) but increased SPB size ($5\ \mu\text{m}$ in diameter).

distance is tunable, demonstrating the potential suitability of the presented approach for the controlled establishment of molecular bridges between SPBs for analyte detection.

The assembly of SPB clusters in the focal point of the underlying domain pattern is further analyzed in **Figure 3a** for different numbers of particles (two, three, four, five, and six SPBs). Singel SPBs are hereby highlighted by red circles. Inferring from the recorded microscope images, the distance between single SPBs is largely reduced within the clustered assembly so that the particles seem to physically touch each other. This emphasizes the

concentrator functionality of the domain pattern design. It was found that the probability of producing a cluster with a specific number of SPBs is highly dependent on the overall bead concentration used for the experiment since this parameter influences the amount of beads entering the focal point. Only cluster formations with a number of SPBs $n \leq 6$ had enough physical space on top of a domain wall within the focal point to be transported within the depicted zigzagging chain structure. For a higher n , three different mechanisms could be observed for the handling of surplus beads: 1.) pushing to an SPB formation following

behind, 2.) dislodging out of the MFL, and 3.) stacking on top of a cluster formation. The latter is visualized in Figure 3b by showing snapshots of the movement of a seven SPB assembly through the focal point. Starting out from a row formation ($t = 0.0$ s), the shortening of domain wall length pushes the SPBs together, until first one ($t = 7.4$ s), then two ($t = 8.6$ s), and finally three SPBs ($t = 11$ s) are ejected to the side of the original SPB row. Upon reaching the focal point, the surplus bead highlighted by a blue circle in Figure 3b jumps on top of the remaining SPB assembly ($t = 14$ s). Once the stripe domain increases, the zigzagging structure is sequentially dissolved back to the original row formation ($t = 20$ s, $t = 22$ s, and $t = 25$ s). The surplus bead rejoins the row formation, maintaining the initial number of seven beads.

The studied system acts as a “magnetophoretic funnel” for transported SPBs: The amount of beads reaching beyond the focal point of the underlying domain pattern is limited by the relation of their sizes to the minimal DW length. For the conducted proof-of-principle experiment with a particle diameter of $2.8 \mu\text{m}$ and a minimal DW length of $5 \mu\text{m}$, 36% of all formations passing through the focal point counted exactly seven SPBs. We note that this statistic is valid only for the investigated set of experimental parameters, including SPB concentration and sample position. The probability that a formation containing a specific number of SPBs is found within the focal point may be increased by adjusting the particle concentration for the applied SPB dispersion.

Varying the number of SPBs and therefore cluster sizes more deterministically, additional experiments were conducted for altered domain pattern dimensions as well as different SPB sizes. A second stripe domain track was designed, following the same architecture of gradually decreasing/increasing domain lengths, but with a lower minimal length of $2 \mu\text{m}$ chosen for the focal point (see Track 2 in Figure S1, Supporting Information). Additionally, the variation of stripe length is much smoother, changing it by $1 \mu\text{m}$ between two consecutive stripes (instead of $5 \mu\text{m}$ for the previously discussed pattern). The positioning and clustering of SPBs with a diameter of $2.8 \mu\text{m}$ above this domain track is visualized in Figure 3c. Similar characteristics are observed: Due to the funnel and concentrator functionality of the pattern design, single SPBs are assembled in chain structures with close physical contact. Since the vertical dimension of the focal point is narrower, clusters with a smaller number of beads are produced. This is reflected by a fraction of 42% accounting for assemblies of only two SPBs measured after leaving the focal point. Figure 3c,d additionally highlights the ejection of surplus beads out of the MFL for large enough SPB formations. These beads are therefore marked with blue circles. Following up the study for modified domain pattern dimensions, another experiment was carried out, this time using micromer-M SPBs (micromod Partikeltechnologie GmbH) with a diameter of $5 \mu\text{m}$ on top of the initially presented domain pattern with a minimal stripe domain length of $5 \mu\text{m}$. As can be seen from Figure 3d, a maximum of three SPBs reached beyond the focal point, with a high ratio of two SPB assemblies present. In fact, 82% of all formations passing through the focal point were left with only two beads. These two additional parameter studies support the capability of the introduced domain pattern design to achieve control over the specific shape of SPB assemblies (row or zigzagging chain) and the number of transported particles (funnel functionality).

2.2.2. Valve Functionality

Upon studying the influence of the external magnetic field pulse duration on the SPBs' transport behavior, another striking feature of the employed magnetic domain pattern was discovered. As known from literature for the utilized magnetic particle transport approach of a dynamically transformed potential energy landscape, SPBs are transiting into a non-linear motion regime (“phase-slipping”) if the frequency of an external rotational magnetic field exceeds a certain critical frequency.^[9] Similarly, SPBs moving above a parallel-stripe domain pattern lose their transportability if the duration of the external magnetic field pulses is too short.^[10] For the here investigated gradually modified stripe domain pattern, a combination of both linear and non-linear particle transport was observed depending on the sample position: At a critical external pulse duration, SPBs present within the focal point of the pattern performed an oscillating motion, “clogging up” the transport track for all approaching particles that are still moving directionally. This observation is visualized in Figure 4 by showing four microscope image snapshots (a-d) of an experiment, where the period of the external magnetic field sequence was chosen to be $T = 80$ ms. As for the previously discussed experiment, the magnitudes of the field pulses stayed at $\mu_0 \cdot H_{z,\text{max}} = \mu_0 \cdot H_{x,\text{max}} = 1$ mT.

Figure 4a shows the start of an experiment, where at $t = 0$ s the SPBs are moving from the right side toward the region of smallest stripe domain length (focal point, located at $x = 100 \mu\text{m}$). For quantification of average SPB positions, gray scale values of the image were averaged along the y -axis and are shown as a function of x -position (brown-filled curve for Figure 4a,b and green-filled curve for Figure 4c,d) within the chosen video frame. Peaks in these lateral intensity profiles represent particle rows forming along the y -axis. When reaching the focal point, the SPBs do not move further but perform oscillating movements around a fixed position. Thus, all other SPBs approaching the focal point were not able to physically pass the stuck particles, leading to highly spatially concentrated aggregates. In the experiment displayed in Figure 4, this has been observed for $t = 1.5$ s (Figure 4b). This behavior is expected to be closely related to a decrease in MFL strength for the smallest stripe domain length (further elaboration on this mechanism in the Discussion section). Upon inverting the phase relation between the magnetic field pulses in z - and x -direction, the SPB transport direction was changed. Now all particles that were previously blocked have been transported away from the focal point. At the same time, new SPBs are moving toward this position from the left side (Figure 4c). At $t = 3.25$ s, also those particles are clogging at the focal point (Figure 4d). In Figure 4e the lateral intensity profiles are plotted as a function of time for the conducted experiment. The progression of each brown line indicates the motion of a single SPB row. Starting from $t = 0$ ms toward $t \approx 500$ ms, diagonal lines are indicating the directed transport of SPBs toward the focal point of the underlying domain pattern. With increasing time, SPBs start to oscillate around a constant x -position with a more blurred distribution of intensity indicating the breakup of distinct particle row formations. At $t \approx 1750$ ms, the phase relation for the external field sequence has been inverted, leading again to diagonal intensity lines that represent the SPB motion from the left to the right. The modified phase relation for the external field pulses

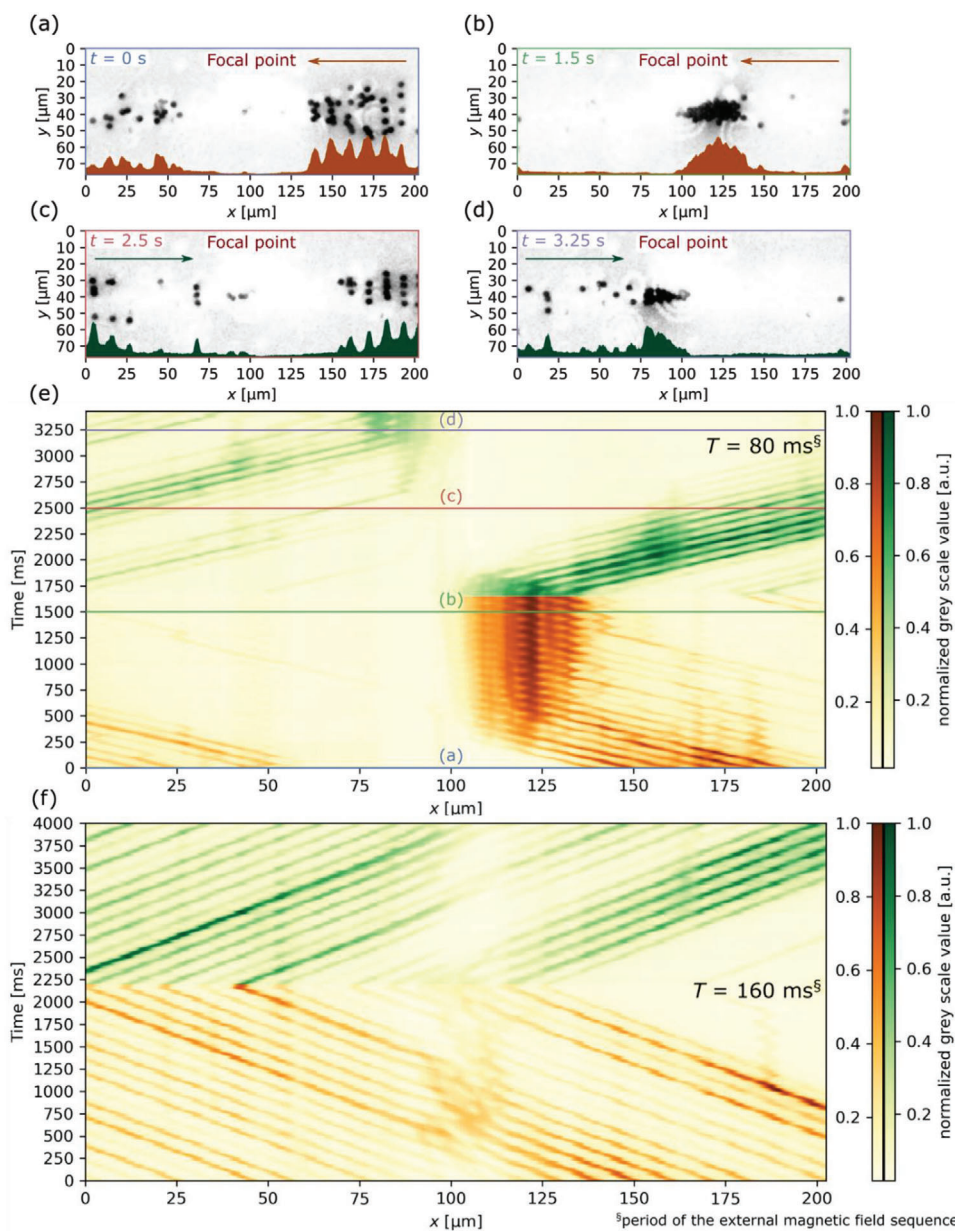


Figure 4. Motion behavior of SPBs above magnetic parallel-stripe domains with gradually decreasing/increasing stripe length when applying a sequence of comparably short magnetic field pulses ($T = 80$ ms). Four exemplary snapshots (a-d) from a transport video recording (with subtracted background) at different experimental times t together with lateral intensity profiles for each frame (brown/green) are shown. Within these profiles, grayscale values of the image were averaged along the y -axis and displayed as a function of x -position. a) SPBs are approaching the focal point of the domain pattern (located in the images at $100 \mu\text{m}$) from the right side and b) are entirely blocked at this position. c,d) Analogous observations were made when SPBs are approaching the focal point from the opposite side. e) Motion dynamics of the particles are visualized by plotting the frame-by-frame lateral intensity profiles of the video recording as a function of time. Colored horizontal lines indicate the times at which frames (a-d) were taken. For comparison, the temporal evolution of lateral intensity profiles for an experiment with longer magnetic field pulses ($T = 160$ ms) is shown in (f). In this case, the blockade of the focal point is lifted and SPBs are passing through. For (e,f), two different color scales (yellow-brown and yellow-green) were used to signify the change in the phase relation between externally applied magnetic field pulses in z - and x -direction, leading to inversion of the transport direction.

and the accompanying change in transport direction is underlined by changing the color scale for the intensity in Figure 4e from yellow-brown to yellow-green. Again, particles perform oscillating movements upon being in proximity to the focal point, most prominently visible between $t \approx 3000$ ms and $t \approx 3500$ ms. In order to compare this “clogged” SPB motion behavior with ex-

periments where full transportability of SPBs was observed (for instance as described in Figure 2), lateral intensity profiles as a function of time are displayed in Figure 4f for a recording obtained when choosing a period $T = 160$ ms for the externally applied magnetic field pulse sequence. As can be seen by the continuous lines (each linked to a moving SPB formation), SPBs are

movable through the focal point for both possible transport directions. Again, the two different color scales (yellow-brown and yellow-green) represent differing phase relations for the external field pulse sequence and the resulting change of transport direction. After testing different periods for the external magnetic field sequence, the “clogging” behavior was observed for $T \leq 120$ ms. This marks the critical pulse time length at which the created magnetophoretic “valve” is closed for incoming SPBs.

3. Discussion

The functional element for magnetophoretic bead transport introduced here is based on a clever design of magnetic domains and combines three functionalities: 1.) An SPB “funnel” for transferring a restricted number of beads per transport step, 2.) an SPB concentrator for bringing single beads into close physical contact, and 3.) an SPB “valve” that can be closed and opened by tuning the frequency of a periodically repeating external magnetic field sequence. The funnel and concentrator functionalities are connected to an observed transformation of SPB rows into SPB clusters upon lateral transport toward the domain pattern’s focal point. Compared to previous results for SPBs assembled above DWs of similar magnetic stripe patterns, this behavior is not intuitively understandable since magnetic moments of the beads are aligned parallel to each other by the effective magnetic field, thereby leading to repulsive dipolar forces between them.^[10] To understand the physical mechanism behind the observed cluster formation, acting forces that are expected to be of major influence were theoretically estimated. These forces include the magnetic force \vec{F}_{mag} in z - and y -direction, the dipolar force \vec{F}_{dip} in dependence on the relative bead positions as well as the electrostatic force \vec{F}_{el} and van der Waals force \vec{F}_{vdW} between SPB surfaces.^[10,39,40] A full description of the force calculations as functions of SPB orientation and separation distance is given in the Supporting Information (see especially Figure S2, Supporting Information). Note that these calculations were solely carried out for Dynabeads M-270 with a diameter of 2.8 μm being captured by the magnetic stray field on top of a DW with 5 μm length.

From the theoretical estimates, it can be inferred that SPB assembly is strongly influenced by the magnetic forces in z - and y -direction. The force in z -direction attracts SPBs toward hh/tt-DW positions^[10,12] and its reach is therefore limited by the DW length. Thus, the smaller the DW length the fewer SPBs can be captured and assembled simultaneously, explaining the funnel functionality of the investigated system. According to the calculations, the strong attraction toward hh/tt-DWs overcomes dipolar repulsion between single SPBs, consequently allowing for the observed decline in SPB separation distance when moving into the domain pattern’s focal point. In addition, the magnetic force in y -direction, which is due to magnetic fringe fields situated at the corners of a stripe domain (see Figure 1c), is expected to contribute further to the stabilization of SPB cluster formations. The zigzagging chain structure for SPBs located at the focal point is supported by an attractive dipolar interaction acting between beads positioned with a displacement in x - and y -directions. As the calculations reveal, an irreversible bead aggregation due to attractive van der Waals forces is hindered due to a stronger repulsive electrostatic force.

From the simulated MFL (see Figure 1c), it is deducible that $|H_z|$ and therefore also the magnetic force is larger for increasing stripe domain length, potentially explaining the SPB motion behavior observed for small external magnetic field pulse lengths, i.e., the particle valve functionality. For a critical pulse length, particles within the focal point, that are exposed to a reduced magnetic force, already transition to the non-linear transport regime while particles at larger stripe lengths with stronger magnetic forces are still linearly transportable. The clogging of SPBs can be physically interpreted as the occurrence of position-dependent critical transition time scales, which is an outstanding feature of the introduced domain pattern design.

4. Conclusion

In this work, a specifically designed magnetic parallel-stripe domain pattern was tailored as a functional LOC element, combining the three functions of particle “funneling”, concentration, and “valve” for superparamagnetic beads (SPBs) in an aqueous medium. Three goals were set for the design of the element: 1.) Introducing a functionality to limit the maximum number of SPBs being transported above the pattern, 2.) bringing SPBs in close proximity to each other, thereby potentially facilitating bead aggregation upon formation of molecular bridges, and 3.) creating an on/off switchable valve for directionally transported SPBs. The domain pattern was engineered to exhibit gradually decreasing/increasing stripe length in a periodic fashion while maintaining a constant stripe width of 5 μm . It was fabricated in an exchange-biased thin film system with in-plane magnetization *via* ion bombardment induced magnetic patterning (IBMP). Magnetic force microscopy (MFM) imaging confirmed the occurrence of the stripe domains with opposite magnetization directions compared to the monodomain environment. Three types of domain walls (DWs) for the different magnetization configurations head-to-head (hh), tail-to-tail (tt), and side-by-side (ss) were identified, representing the sources for the magnetic stray field landscape (MFL) that is an essential component of the utilized particle transport concept. Spatial components of the MFL were simulated based on micromagnetic calculations for the domain pattern, revealing the field in z -direction above the center of a hh/tt DW to be the strongest, while additional field components in y -direction are expected as compared to previously investigated parallel-stripe domain patterns.^[10] After adding an aqueous dispersion of Dynabeads M-270 (diameter of 2.8 μm) above the substrate, directed transport of the particles was initialized by applying external trapezoidal magnetic field pulses in z - and x -direction. As a striking feature of the observed motion behavior, formations of SPBs that started out as vertical rows were transformed into cluster formations with a zigzagging arrangement of single particles upon reaching the sample area with smallest stripe domain length (focal point). This cluster formation has been reversibly turned back to the original row formation when leaving the focal point toward regions with increasing stripe domain length. Although the amount of SPBs arriving at the focal point is statistically distributed, it was determined that 36% of all clusters leaving the focal point contained exactly seven beads. Modifying the domain pattern dimensions as well as the size of transported SPBs, 42%, and 82%, respectively, of all clusters leaving the focal point counted exactly two

SPBs. This observation demonstrates further the possibility of producing magnetic bead aggregates with a defined number of particles. The revealed funnel functionality of the domain pattern design paves the way for a variety of applications, where a defined number of magnetic particles is needed at a designated chip area, e.g., the calibration of magnetoresistive sensor elements for magnetic particle detection. Studying the influence of the external magnetic field pulse length, a transition toward a blocked focal point was observed, i.e., passing of the SPBs through the focal point was inhibited by non-transportable beads stuck within the focal point. This showcases the particle “valve” functionality of the investigated transport system, with the external magnetic field pulse length being the lever to open or close the valve. Within a quantitative theoretical discussion, the main contributing forces on the SPBs were calculated to provide physical explanations for the observed particle clustering/de-clustering behavior. It was discovered that the magnetic force acting perpendicular to the substrate plane (z-direction) alongside occurring fringe fields at the upper/lower borders of magnetic stripe domains are most likely promoting the observed densely packed SPB cluster formations within the magnetic pattern’s focal point. For larger stripe domain lengths, repulsive magnetostatic forces between single SPBs lead to the observed vertical row arrangements with approximately equal spacing between the particles. Combining the SPB motion concept presented within this work with adequately surface-functionalized particles, analyte detection based on induced irreversible particle aggregation is a promising application for LOC systems. The aggregate size and shape (defined by the number of aggregated beads) are hereby adjustable *via* the minimum stripe domain length as well as the particle size and concentration, making this “magnetophoretic funnel” especially potent for controllably assembling 3D structures in a liquid environment on top of a flat chip substrate.

5. Experimental Section

Fabrication of Magnetically Patterned Transport Substrate: The magnetic parallel-stripe domain pattern with gradually decreasing/increasing stripe length (stripe width of 5 μm) was obtained via IBMP^[20,23] of an EB thin film system. A $\text{Cu}^{5\text{ nm}}/\text{Ir}_{17}\text{Mn}_{83}^{30\text{ nm}}/\text{Co}_{70}\text{Fe}_{30}^{10\text{ nm}}/\text{Si}^{20\text{ nm}}$ layer stack was deposited onto a naturally oxidized Si (100) wafer piece (ca. 1 cm \times 1 cm) by rf-sputtering at room temperature. Subsequently, the sample was subjected to a field cooling procedure to induce the in-plane direction of the EB. Therefore, the sample was annealed in a vacuum chamber (base pressure = 5×10^{-7} mbar) at 300 $^{\circ}\text{C}$ for 60 min in an in-plane magnetic field of 145 mT. For IBMP, a photoresist with a sufficient thickness to prevent 10 keV He ions from penetrating the magnetic layer system, was deposited on the sample surface via spin coating. The photoresist was structured to exhibit 5 μm wide stripe gaps with a 5 μm separation of adjacent stripes and a periodically repeating decrease/increase of the stripe length (see Figure S1, Supporting Information for an image of the resulting resist structure). For Track 1 the stripe length was varied between 50 μm and 5 μm with an increment of 5 μm between adjacent stripes (except for the 50 μm and 5 μm long stripes, which were repeated once before subsequent length modulation). In the case of Track 2, the stripe length was modulated between 25 μm and 2 μm using an increment of 1 μm (here 25 μm and 2 μm long stripes were also repeated once). The long axis of the stripes was positioned perpendicular to the initial EB direction (set by the field cooling procedure). Structuring of the resist was performed by utilizing direct laser writing lithography. Next, the sample was bombarded with a dose of 1×10^{15} cm^{-2} He ions (kinetic energy of 10 keV) using a home-built Penning ion source. For an antiparallel stripe magnetization

with respect to the surrounding (protected by the resist layer), an in-plane homogenous magnetic field (100 mT) was applied antiparallel to the initial EB direction during ion bombardment. Afterward, the photoresist was removed by washing the sample several times with acetone. Then the surface was cleaned by rinsing the sample with acetone, isopropanol, and water. After drying, a 200 nm thick PMMA layer was deposited on top of the sample by spin coating.

Particle Transport: For inducing SPB motion, a home-built setup consisting of orthogonally placed Helmholtz coil pairs was used for the application of trapezoidal magnetic field pulses in z- and x-direction, i.e., perpendicular and parallel to the transport substrate plane. Each pulse consisted of a linear rising time for the magnetic field, a plateau time, and a linear drop time, with the pulse direction being periodically alternated between H_{max} and $-H_{\text{max}}$. The duration of pulse rising and drop times was given by the pulse magnitude and the alteration rate of the external magnetic field

($3.2 \cdot 10^6 \text{ Am}^{-1}\text{s}^{-1}$). The pulse magnitude was chosen to be $\mu_0 \cdot |H_{\text{max},x}| = \mu_0 \cdot |H_{\text{max},z}| = 1 \text{ mT}$ and a temporal phase shift of $\pi/2$ between pulse sequences in z- and x-direction were applied. Before initializing the transport experiment, a volume of 20 μL of a diluted dispersion of SPBs (Dynabeads M-270 Carboxylic Acid^[41] or micromer-M^[42]) was pipetted into a microfluidic chamber adhered to the top of the magnetically patterned substrate. The chamber was fabricated by cutting a window of approximately 8 mm \times 8 mm into a Parafilm sheet that was of the substrate’s size. After sealing the chamber with a square-shaped glass cover slip, the transport substrate was placed in the middle of the Helmholtz coil arrangement with the substrate plane positioned perpendicular to the external z-field and in-plane domain magnetization direction positioned parallel to the external x-field. Approaching the sample with an optical bright field microscope (40 \times magnification objective, N.A. = 0.6), SPB motion was recorded with an attached high speed camera. Qualitative analysis was carried out by using a Mikrotrotron EoSens CoaXPress CXP-6 camera (maximum resolution of 4096 px \times 3072 px) at a framerate of 25 frames per second (fps) and quantitative analysis was achieved by using an Optonics CR450 \times 2 camera (maximum resolution of 800 px \times 600 px) at a framerate of 1000 fps.

Micromagnetic Simulations: The simulation package MuMax3^[37] was utilized to compute the magnetization distribution $\vec{m}(x, y)$ within a region of interest (see black rectangle in Figure 1b) for the investigated stripe domain pattern with gradually modified stripe length. Two regions were defined for areas of the sample that were treated/untreated by He ion bombardment: The stripes themselves were ion bombarded and the surrounding environment was untreated. Depending on this categorization, differing magnetic properties were assigned: An exchange stiffness constant of $A_{\text{ex}} = 3 \cdot 10^{-11} \frac{\text{J}}{\text{m}}$ ^[43] a saturation magnetization of $M_{\text{S}} = 1.23 \cdot 10^6 \frac{\text{A}}{\text{m}}$ ^[44] a uniaxial anisotropy constant of $K = 4.5 \cdot 10^4 \frac{\text{J}}{\text{m}^3}$ ^[36] for the non-bombarded environment, and accordingly $A_{\text{ex}} = 3 \cdot 10^{-11} \frac{\text{J}}{\text{m}}$, $M_{\text{S}} = 1.18 \cdot 10^6 \frac{\text{A}}{\text{m}}$, $K = 3.375 \cdot 10^4 \frac{\text{J}}{\text{m}^3}$ for the bombarded stripes. Note that the values for saturation magnetization and anisotropy constant were slightly reduced for the bombarded region as uncovered by previous investigations.^[44,45] For implementing the exchange bias-related pinning of the respective domain magnetizations, additional biasing magnetic fields were defined for bombarded/non-bombarded areas with opposing directions. Here, the magnetic flux densities were chosen to be 13 mT for the non-bombarded regions and 6.7 mT for bombarded regions according to experimentally determined values from hysteresis loop measurements. The region of interest (20.48 μm \times 40.96 μm) was discretized into cubic elements of 5 nm \times 5 nm \times 10 nm sizes and the simulation software computed the relaxed magnetization state of the described system, which was subsequently used for obtaining magnetic stray field components (see Figure 1c) via a dipole approximation.

Supporting Information

Supporting Information is available from the Wiley Online Library or from the author.

Acknowledgements

Fruitful discussions with M. Vogel are gratefully acknowledged.
Open access funding enabled and organized by Projekt DEAL.

Conflict of Interest

The authors declare no conflict of interest.

Author Contributions

R.H. performed the investigation, formal analysis, and wrote the original draft. L.P. performed the investigation, formal analysis, and reviewed/edited the manuscript. M.M. performed the formal analysis. P.K. performed the investigation, acquired resources, and reviewed/edited the manuscript. A.E. performed the supervision, conceptualization, project administration, funding acquisition, and reviewed/edited the manuscript.

Data Availability Statement

The data that support the findings of this study are available from the corresponding author upon reasonable request.

Keywords

ion bombardment induced magnetic patterning, lab-on-a-chip, magnetic domain engineering, magnetic field landscapes, magnetic particle transport, superparamagnetic beads

Received: July 6, 2023

Revised: September 25, 2023

Published online: October 27, 2023

-
- [1] M. A. M. Gijs, *Microfluid. Nanofluid.* **2004**, *1*, 22.
 [2] N. Pamme, *Lab Chip* **2006**, *6*, 24.
 [3] C. Ruffert, *Micromachines* **2016**, *7*, 21.
 [4] L. J. Kricka, *Clin. Chim. Acta* **2001**, *307*, 219.
 [5] A. Manz, N. Graber, H. M. Widmer, *Sens. Actuators B: Chem.* **1990**, *1*, 244.
 [6] J. Knight, *Nature* **2002**, *418*, 474.
 [7] A. Van Reenen, A. M. De Jong, J. M. Den Toonder, M. W. Prins, *Lab on a Chip* **2014**, *14*, 1966.
 [8] C. P. Moerland, L. J. Van Ijzendoorn, M. W. J. Prins, *Lab Chip* **2019**, *19*, 919.
 [9] S. Rampini, P. Li, G. U. Lee, *Lab Chip* **2016**, *16*, 3645.
 [10] D. Holzinger, I. Koch, S. Burgard, A. Ehresmann, *ACS Nano* **2015**, *9*, 7323.
 [11] R. Abedini-Nassab, M. Pouryosef Miandoab, M. Sasmaz, *Micromachines* **2021**, *12*, 768.
 [12] M. Reginka, H. Hoang, Ö. Efendi, M. Merkel, R. Huhnstock, D. Holzinger, K. Dingel, B. Sick, D. Bertinetti, F. W. Herberg, A. Ehresmann, *Langmuir* **2021**, *37*, 8498.
 [13] R. Huhnstock, M. Reginka, A. Tomita, M. Merkel, K. Dingel, D. Holzinger, B. Sick, M. Vogel, A. Ehresmann, *Sci. Rep.* **2021**, *11*, 21794.
 [14] A. Chen, T. Byvank, G. B. Vieira, R. Sooryakumar, *IEEE Trans. Magn.* **2013**, *49*, 300.
 [15] A. Sarella, A. Torti, M. Donolato, M. Pancaldi, P. Vavassori, *Adv. Mater.* **2014**, *26*, 2384.
 [16] U. Sajjad, F. Klingbeil, F. Block, R. B. Holländer, S. Bhatti, E. Lage, J. Mccord, *Lab Chip* **2021**, *21*, 3174.
 [17] B. Lim, P. Vavassori, R. Sooryakumar, C. Kim, *J. Phys. D: Appl. Phys.* **2017**, *50*, 033002.
 [18] P. Tierno, F. Sagués, T. H. Johansen, T. M. Fischer, *Phys. Chem. Chem. Phys.* **2009**, *11*, 9615.
 [19] A. Ehresmann, D. Lengemann, T. Weis, A. Albrecht, J. Langfahl-Klabes, F. Göllner, D. Engel, *Adv. Mater.* **2011**, *23*, 5568.
 [20] A. Ehresmann, I. Koch, D. Holzinger, *Sensors* **2015**, *15*, 28854.
 [21] M. Urbaniak, M. Matczak, G. D. Chaves-O'flynn, M. Reginka, A. Ehresmann, P. Kuswik, *J. Magn. Magn. Mater.* **2021**, *519*, 167454.
 [22] A. Mougin, S. Poppe, J. Fassbender, B. Hillebrands, G. Faini, U. Ebels, M. Jung, D. Engel, A. Ehresmann, H. Schmoranz, *J. Appl. Phys.* **2001**, *89*, 6606.
 [23] A. Ehresmann, I. Krug, A. Kronenberger, A. Ehlers, D. Engel, *J. Magn. Magn. Mater.* **2004**, *280*, 369.
 [24] P. Kuswik, A. Ehresmann, M. Tekielak, B. Szymanski, I. Sveklo, P. Mazalski, D. Engel, J. Kisielewski, D. Lengemann, M. Urbaniak, C. Schmidt, A. Maziewski, F. Stobiecki, *Nanotechnology* **2011**, *22*, 095302.
 [25] E. Albisetti, D. Petti, M. Pancaldi, M. Madami, S. Tacchi, J. Curtis, W. P. King, A. Papp, G. Csaba, W. Porod, P. Vavassori, E. Riedo, R. Bertacco, *Nat. Nanotechnol.* **2016**, *11*, 545.
 [26] I. Berthold, U. Löschner, J. Schille, R. Ebert, H. Exner, *Phys. Procedia* **2014**, *56*, 1136.
 [27] T. Ueltzhöffer, R. Streubel, I. Koch, D. Holzinger, D. Makarov, O. G. Schmidt, A. Ehresmann, A. C. S. Nano, *ACS Nano* **2016**, *10*, 8491.
 [28] B. Lim, S. R. Torati, K. W. Kim, X. Hu, V. Reddy, C. Kim, *NPG Asia Mater.* **2017**, *9*, e369.
 [29] C. P. Gooneratne, I. Giouroudi, C. Liang, J. Kosel, *J. Appl. Phys.* **2011**, *109*, 07E517.
 [30] C. Gooneratne, R. Kodzius, F. Li, I. Foulds, J. Kosel, *Sensors* **2016**, *16*, 1369.
 [31] M. Urbaniak, D. Holzinger, A. Ehresmann, F. Stobiecki, *Biomicrofluidics* **2018**, *12*, 044117.
 [32] P. Li, D. Gandhi, M. Mutas, Y.-F. Ran, M. Carr, S. Rampini, W. Hall, G. U. Lee, *Nanoscale* **2020**, *12*, 3482.
 [33] R. Wirix-Speetjens, G. Reekmans, R. De Palma, C. Liu, W. Laureyn, G. Borghs, *Sens. Actuators B Chem.* **2007**, *128*, 1.
 [34] S. Rampini, P. Li, D. Gandhi, M. Mutas, Y. F. Ran, M. Carr, G. U. Lee, *Sci. Rep.* **2021**, *11*, 5302.
 [35] Y.-F. Ran, C. Fields, J. Muzard, V. Liauchuk, M. Carr, W. Hall, G. U. Lee, *Analyst* **2014**, *139*, 6126.
 [36] D. Holzinger, N. Zingsem, I. Koch, A. Gaul, M. Fohler, C. Schmidt, A. Ehresmann, *J. Appl. Phys.* **2013**, *114*, 013908.
 [37] A. Vansteenkiste, J. Leliaert, M. Dvornik, M. Helsen, F. Garcia-Sanchez, B. Van Waeyenberge, *AIP Adv.* **2014**, *4*, 107133.
 [38] W. Nolting, *Grundkurs Theoretische Physik 3*, Springer, Berlin **2013**.
 [39] J. N. Israelachvili, *Intermolecular and Surface Forces*, Academic Press, Cambridge, Massachusetts **2011**.
 [40] I. Koch, M. Langner, D. Holzinger, M. Merkel, M. Reginka, R. Huhnstock, A. Tomita, C. Jauregui Caballero, A. Greiner, A. Ehresmann, *Part. Part. Syst. Charact.* **2021**, *38*, 2100072.
 [41] Thermofisher, "Dynabeads M-270 Carboxylic Acid," <https://www.thermofisher.com> (accessed: March 2023).
 [42] Micromod, "Micromer-M", <https://micromod.de/en/product-category/magnetic-particles/micromer-m-magnetic-particles/> (accessed: September 2023).
 [43] D. V. Berkov, C. T. Boone, I. N. Krivorotov, *Phys. Rev. B Condens. Matter Mater. Phys.* **2011**, *83*, 54420.
 [44] H. Huckfeldt, A. Gaul, N. D. Möglich, D. Holzinger, D. Nissen, M. Albrecht, D. Emmrich, A. Beyer, A. Gölzhäuser, A. Ehresmann, *J. Phys.: Condens. Matter* **2017**, *29*, 125801.
 [45] N. D. Möglich, M. Merkel, A. Gaul, M. Meyl, G. Götz, G. Reiss, T. Kuschel, A. Ehresmann, *New J. Phys.* **2018**, *20*, 053018.